Asian Journal of Chemistry; Vol. 33, No. 11 (2021), 2831-2838

ASIAN JOURNAL OF CHEMISTRY

https://doi.org/10.14233/ajchem.2021.23416

Synthesis and Characterization of Nickel Cobalt Vanadate ($NiCo_2V_2O_8$) Nanostructures: Photocatalytic and Supercapacitor Applications

LAKSHMANA NAIK R.[1,*], T. BALA NARSAIAH[1], C.R. RAVIKUMAR[2], A. NAVEEN KUMAR[2], K. VINUTHA[2], A.A. JAHAGIRDAR[3] and H.C. ANANDA MURTHY[4]

[1]Department of Chemical Engineering, JNTUA College of Engineering Anantapur, Ananthapuramu-515002, India
[2]Research Center, Department of Science, East West Institute of Technology, VTU, Bengaluru-560091, India
[3]Department of Chemistry, Ambedkar Institute of Technology, Bangalore, 560056, India
[4]Department of Applied Chemistry, School of Applied Natural Science, Adama Science and Technology University, Adama, Ethiopia

*Corresponding authors: E-mail: lakshman2027@gmail.com

Received: 16 July 2021; *Accepted*: 15 September 2021; *Published online*: 20 October 2021; AJC-20571

With the emerging newer energy storage applications, transition metal vanadates are booming up as better catalysts. Among all the transition metal vanadates, nickel cobalt vanadate nanomaterials ($NiCo_2V_2O_8$ NP), are being considered as a promising material with electrocatalytic and photocatalytic activity. In this article, the synthesis of circular and ovular structured $NiCo_2V_2O_8$ nanostructures by the hydrothermal route without using any capping agent is reported. The crystallinity, physical structure and morphology of the prepared nanomaterial were studied by X-ray diffraction (XRD), transmission electron microscopy (TEM) and Fourier transform infrared (FT-IR) spectroscopy. The photocatalytic property of $NiCo_2V_2O_8$ nanostructures was studied by decolorizing industrially hazardous dye such as malachite green dye under ultra-violet light conditions for a regular interval of time (10 min) up to 60 min. The experiments showed decolorization efficiencies as 52.43 for malachite green dye. The electrochemical behaviour of the prepared compound was studied and energy specific capacity was elucidated as 218.4 F g^{-1} with high reversibility property the material. The $NiCo_2V_2O_8$ nanostructures showed better electrochemical activity and photocatalytic activity, which could be utilized for supercapacitor and pollutant remediation applications.

Keywords: $NiCo_2V_2O_8$ nano structures, Photocatalysis, Dye degradation, Malachite green, Supercapacitor, Specific capacity.

INTRODUCTION

In recent years, due to the enormous growth in the world population, the demand and supply of energy resources has been found to increase significantly and believed to play a key role in the economic, industrial and overall growth of the country. The necessity of the energy by man continues to increase with time. Presently, energy requirements of the society energy are collectively met by the fossils fuels, hydropower, geothermal power, wind power, *etc.*, but the storage of energy still remains a challenge and not economical which attracts scientists to work on the efficient utilization of energy [1]. There are various ways in which energy can be stored [2,3]. Among many ways, supercapacitors are the new avenue in energy storage and lied forefront of the environmentally healthy electrochemical energy storage systems compared to traditional batteries, which are linked to pollution [4,5]. Based on the working mechanisms supercapacitors are broadly grouped in two classes such as electrical double layered capacitors (EDLCs) and pseudo capacitors (PCs). The EDLCs electrode material mainly contains carbon whereas the PCs electrode includes metal oxides and metal hydroxide conducting polymers [6]. The most common material utilized for PCs electrode is ruthenium oxide due to its capacitance properties through fast reversible multielectron surface faradic redox reactions. Eventually, there has been a mounting attention in transition metal oxides due to their augmented combination, diverse morphological features and crystallinity related electrode resources for energy storage and generation devices [7]. It has led to the rising curiosity in the electrochemical effectiveness and purification of water by nanostructures of metal oxide to be used as catalyst for both anode and cathode. For many areas of human life, their unique

size-dependent characteristics make these materials essential and outstanding. Nickel is one of the most valuable transition metals found in the Earth's crust and the cornerstone of modern infrastructure. In recent years, in light of their essential and technological aspects, nickel metal oxides have become the focus of the investigation. $NiCo_2V_2O_8$ is an excellent catalyst among many transition metal oxides and several basic researches on catalytic oxidation have also been reported [8]. Among these, vanadium generates several oxygen compounds; they have various optical, structural and chemical properties. The major property variations between various phases of vanadium oxides relay on their arrangement that defines certain characteristics [9]. A significant number of vanadium oxide nanostructures, including nanorods, nanobelts and nanowires, were examined for their usage as electrode materials [10]. Vanadium nanotubes offer an ability to use metal cation vanadium oxide to increase the electrochemical productivity of a nanostructure.

At the present time, advanced specific capacitance values were shown by ternary metal oxides pseudo capacitors due to the fact that ternary metal oxides triple oxide states, outstanding electrical conduction and outstanding electrochemical behaviour described previous $Zn_3V_2O_8$, $CoMoO_4$ and $ZnFe_2O_4$. Vanadium oxide (VO_x) based electrode materials as both cathode and anode for Li-ion batteries have got attention in the field due to their good crystallinity and varied morphologies. Different electrochemical behaviours have displayed by the vanadium oxide due to its multivalent nature [11,12].

The present work reports the preparation of $NiCo_2V_2O_8$ nanostructures by the simple hydrothermal route. The photocatalytic activity (PCA) of the nanostructures was performed on malachite green dye under UV light irradiation at a regular interval of time. The prepared $NiCo_2V_2O_8$ were characterized for crystallinity, phase, structural and morphological properties using advanced analytical tools. The detailed study of super capacitive property of $NiCo_2V_2O_8$ electrode material has been performed in 0.1 M HCl using cyclic voltammetry (CV) and electrochemical impedance spectroscopy (EIS) and charge-discharge techniques. This work intends to utilize the photocatalytic and electrochemical studies of $NiCo_2V_2O_8$ nanomaterials for broad spectrum of energy and water treatment applications to explore the eco-friendly, sustainable, scalable and cleaner methodologies for the better tomorrow.

EXPERIMENTAL

All the chemicals were purchased from Sigma-Aldrich, analytical grade and arrangement (solutions) were set up by using double-distilled water. Ammonium metavanadate (NH_4VO_3), *N*-methyl-2-pyrrolidone, urea, cobalt nitrate and nickel nitrate and ethanol.

Preparation of $NiCo_2V_2O_8$ nanomaterial: $NiCo_2V_2O_8$ nanomaterial was synthesized by a simple hydrothermal method. In a typical procedure, 1.323 g of ammonium metavanadate (NH_4VO_3) was added to solution containing 87.5 mL of *N*-methyl-2-pyrrolidone with constant magnetic stirring for 1 h (solution A). To above solution A, 8.450 g of urea were added with constant stirring and then nickel nitrate (1.678 g) and cobalt nitrate (3.292 g) were added into 250 mL water (solution B). Then, the solution B was mixed with the solution A slowly with continuous stirring. Finally, the whole solution was made up to 350 mL and transferred to Teflon lined autoclave and heat treated at 160 ºC for 36 h. In the wake of being cooled to encompassing temperature normally, the powder in the autoclave was gathered by centrifugation, washed with deionized water, trailed by total ethanol multiple times and dried at 80 ºC for 12 h. At last, the dried material was calcined in air at 450 ºC for 3 h with a heating rate of 2 ºC per min^{-1} to acquire exceptionally crystalline powders. The calcined sample was used for further characterization.

RESULTS AND DISCUSSION

XRD studies: Fig. 1 depicts the XRD pattern of hydrothermally synthesized crystalline $NiCo_2V_2O_8$ nanostructure. The appearance of the most prominent peaks corresponding to the planes, (131), (221), (151), (244) is in compliance with the standard pattern as mentioned in JCPDS card no. 74-1487 space [13] group *Cmca* without any impurity with a = 5.928 Å, b = 11.378 Å, c = 8.245 Å, density (ρ) = 4.86 Mg m^{-3}. Orthorhombic (space group *Cmca*) lattices result from the stretching of a cubic lattice along 2 of its orthogonal pairs by 2 different factors a/b (0.52) and b/c or c/a = 1.38 resulting in a rectangular prism with different lattice parameters (a, b and c) as tabulated in Table-1.

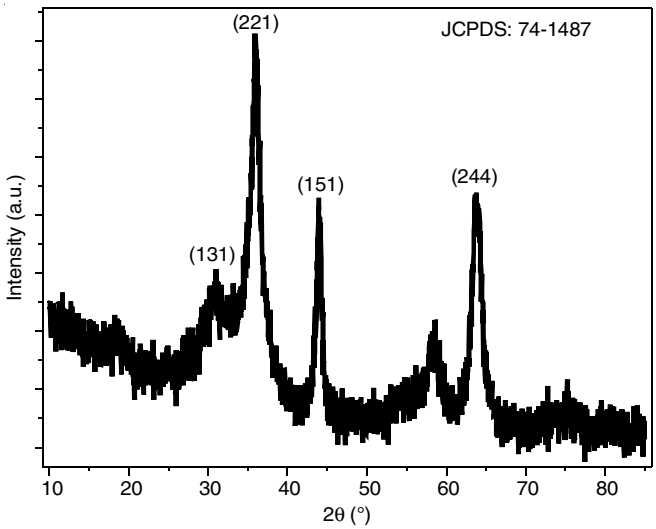

Fig. 1. XRD pattern of $NiCo_2V_2O_8$ nano structures

TABLE-1
LATTICE PARAMETERS OF $Ni_3Co_2V_2O_8$ NANO STRUCTURE

a (Å)	B (Å)	c (Å)	α = β = γ	a/b	b/c	c/a	V (Å^3)	D (nm) for plane (151)
5.928	11.378	8.245	90°	0.52	1.38	1.38	555.52	9.04

Space group: Cmca; Structure: orthorhombic

Using Scherrer's equation (eqn. 1) [14]:

$$D = \frac{k\lambda}{\beta\cos\theta} \quad (1)$$

the average crystallite size was deduced to be 9.04 nm for the plane ((151) peak at $2\theta = 44°$), where, k = diffraction constant (0.9), X-ray wavelength (λ) = 1.54×10^{-10} m, D = crystallite size, β = full-width half-maximum (FWHM), θ = diffraction angle on X-ray incidence.

FTIR studies: The recorded FTIR spectrum of prepared $NiCo_2V_2O_8$ nanostructure is depicted in Fig. 2. The bands observed between the range 500 to 1000 cm^{-1} can be assigned to V-O and V=O stretching and bending vibrations, respectively. The broad band beginning at 3500 cm^{-1} is possibly due to O-H vibration of adsorbed water over $NiCo_2V_2O_8$ nanostructures. The major patterns in the ragne of 1650-1460 and 2930-2850 cm^{-1} were subjected to O–H bending and stretching vibrations, respectively [15]. From Fig. 3a-b, SEM images of $NiCo_2V_2O_8$ depicted differently sized nanostructures. Nearly spherical and irregular geometries were also presented in Fig. 3a-b for the nanostructures. In addition, the $NiCo_2V_2O_8$ nanostructures were found to have been agglomerated (Fig. 3a) and exhibited hexagonal disc-like structures (Fig. 3b) with average diameters of around 20 nm.

Fig. 4 depicts the energy gap (E_g) spectrum with inset figure showing the diffused reflectance spectrum of $NiCo_2V_2O_8$ nanostructures. Kubelka-Munk (KM) equation (eqns. 2 & 3) was used to calculate the E_g value and found to be 2.37 eV.

$$F(R) = \frac{(1-R)^2}{2R} \quad (2)$$

$$F(R)h\nu = A(h\nu - E_g)^n \quad (3)$$

where, F(R) is the function absolute reflection (R) also called as Kubelka-Munk function, A and hν are constant and an

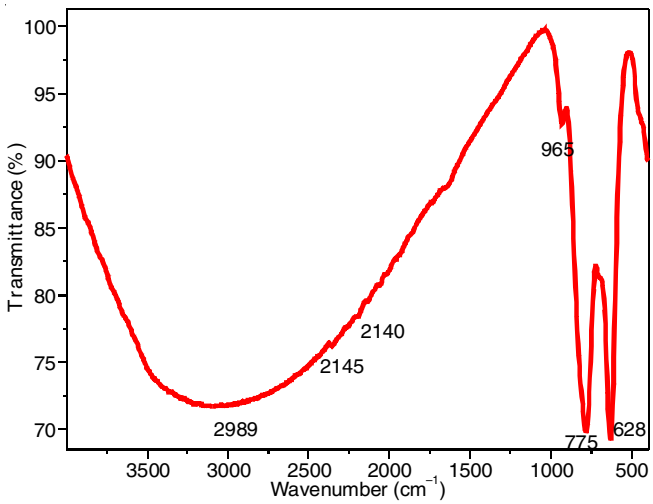

Fig. 2. The FT-IR spectrum of $NiCo_2V_2O_8$ nano structures

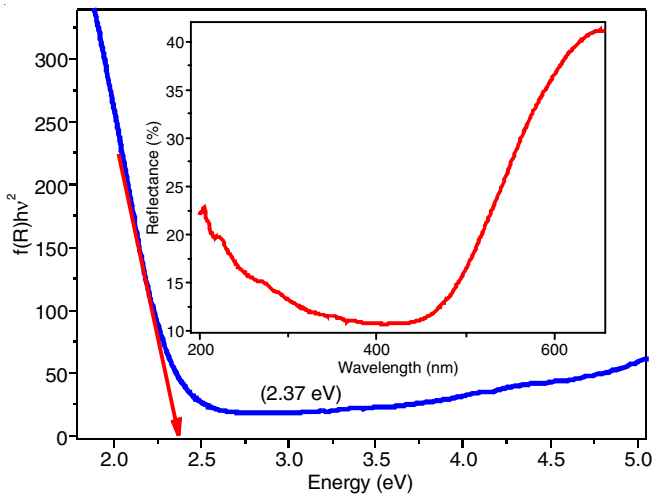

Fig. 4. Band gap and diffused reflectance spectra (inset) of $NiCo_2V_2O_8$ nano structures

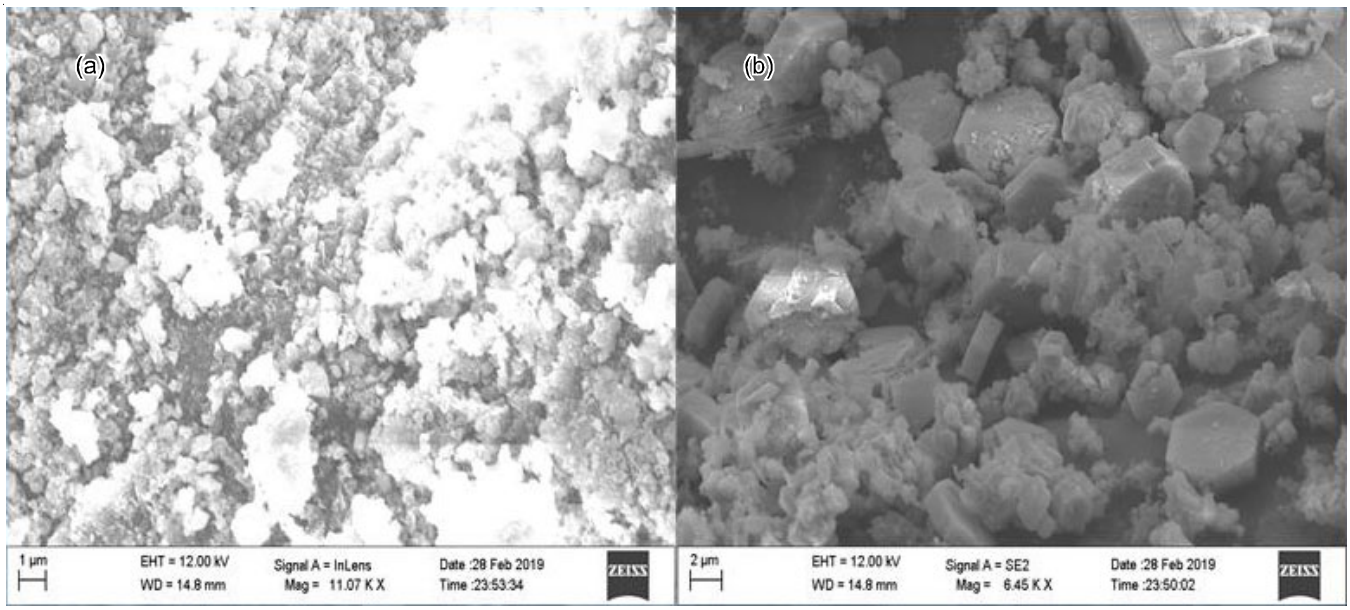

Fig. 3. SEM images of $NiCo_2V_2O_8$ nano structures (a and b)

energy of the photon for n = 2, direct allowed transition and n = ½, indirectly allowed transition [16,17].

TEM studies: Transmission electron microscopic images showed circular and ovular $NiCo_2V_2O_8$ nanostructures and the size slightly varies in the range between 5 nm to 50 nm (Fig. 5a-b). In addition, the particles of $NiCo_2V_2O_8$ appears to agglomerate showing high surface charge as well as surface activity. The SAED (selected area electron diffraction) pattern confirms the polycrystallinity of the nanomaterial whereas all the bright rings (Fig. 5c) correspond to different planes in the prepared $NiCo_2V_2O_8$ material. Fig. 5d shows the different crystal planes justifying the formation of the crystalline structure.

Photocatalytic study: All the experiments were conducted in a photocatalytic glass reactor with malachite green as model dye and $NiCo_2V_2O_8$ as the photocatalyst. In these experiments, synthesized $NiCo_2V_2O_8$ (60 mg) was thoroughly mixed with a 20 ppm dye solution using a magnetic stirrer. To investigate dye decolorization, 5 mL of dye solution was taken out every 15 min, centrifuged and analyzed with a UV-Vis instrument using the characteristic adsorption band at 511 nm. Fig. 6a shows the UV-vis absorption spectral changes observed during photodecalorization of malachite green dye by the prepared $NiCo_2V_2O_8$ nanocatalyst. It is important to note that the prepared nanocatalyst exhibited a higher photocatalytic activity when

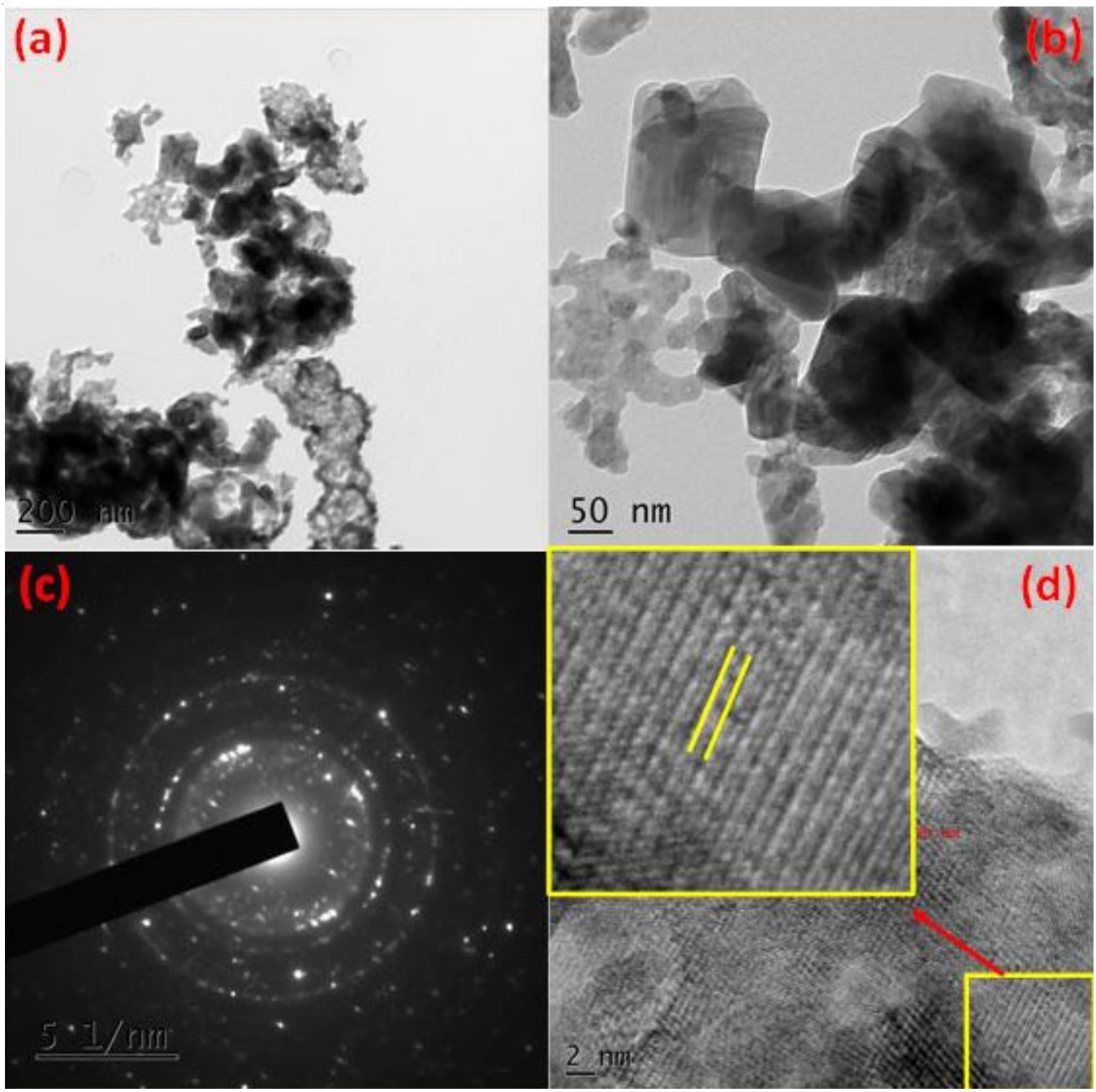

Fig. 5. TEM images (a) micrographs at magnification of 200 nm (b) 50 nm (c) selected area emission diffraction (SAED) and (d) high resolution (HR)-TEM image showing different planes of $NiCo_2V_2O_8$ material

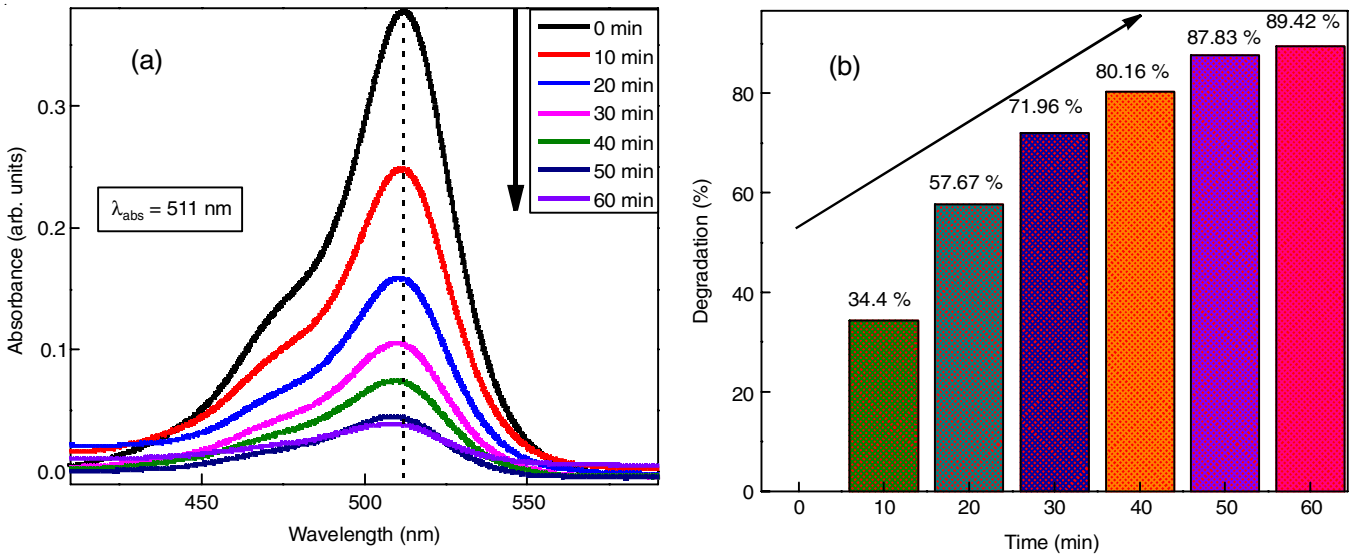

Fig. 6. (a) Absorption spectra of decomposition of malachite green by $NiCo_2V_2O_8$, (b) Percentage decomposition of malachite green dye over $NiCo_2V_2O_8$

exposed to UV radiation. At 511 nm, as can be seen from the UV-visible absorption spectra (Fig. 6a), a gradually decreases during the photocatalytic decolorization for malachite green respectively, as the UV light illumination time interval was increased. This probably might be because malachite green normally degrade due to the complete cleavage of conjugated chromophore [18,19]. The largest absorption band decreases sharply, indicating that malachite green dye becomes nearly colourless.

The absorbance peaks decrease gradually with the irradiation time as the solution was irradiated with UV light ($\lambda = 254$ nm) along with the catalyst, confirming the enhanced photocatalytic activity of $NiCo_2V_2O_8$ nanomaterial. The decrease in the intensity of the absorption peak for malachite green occurred rapidly during the preliminary phase of the contact period, but became delayed as the system gradually reached the equilibrium. The rapid degradation at first can be attributed to the abundance of active sites on the catalyst, but decolorization became less preferred after a certain time due to the occupation of these sites [19,20]. The percentage of degradation for malachite green dye over $NiCo_2V_2O_8$ was calculated using the eqn. 4 and found to be 89.42.

$$\text{Degradation (\%)} = \frac{C_o - C_e}{C_o} \times 100 \quad (4)$$

where, C_o is the initial dye concentration and C_e is the dye concentration after photo-decolorization at time per seconds. Fig. 6b display a plot of percent dye degradation *versus* irradiation time for synthesized $NiCo_2V_2O_8$. The graphs show that malachite green dye had a higher percent of degradation. The kinetic reviews of the decolorization of malachite green dye over $NiCo_2V_2O_8$ photocatalyst are shown in Table-2.

According to the values, the PC reactions of malachite green dye on the $NiCo_2V_2O_8$ sample adopt pseudo-first-order kinetics, which is in consistent with the Langmuir-Hinshelwood model (eqn. 5) [20].

$$\ln\left(\frac{C}{C_o}\right) = kt \quad (5)$$

TABLE-2
KINETIC REVIEWS OF THE DECOLORIZATION OF MALACHITE GREEN DYE OVER $NiCo_2V_2O_8$ NANO STRUCTURES

t	C	c/c_o	log c/c_o	-log c/c_o	D (%)
0	20	1	0	0	0
10	13.12	0.65600	-0.18310	0.183096	34.400
20	8.465	0.42325	-0.37340	0.373403	57.675
30	5.608	0.28040	-0.55222	0.552222	71.960
40	3.968	0.19840	-0.70246	0.702458	80.160
50	2.433	0.12165	-0.91489	0.914888	87.835
60	2.116	0.10580	-0.97551	0.975514	89.420

The outcome clearly established that the k value for malachite green dye reaches the maximum.

A graph of C/C_o *versus* time under UV light irradiation is presented in Fig. 7a. Fig. 7b shows the dye degradation half-life time, with 50% degradation of dye observed over 16.91 min for malachite green dye. The obtained result showed that $NiCo_2V_2O_8$ behaved as excellent photocatalyst for decolouration of malachite green dye. $NiCo_2V_2O_8$ nanostructures were found to have boosted the efficiency by way of production of more number of free electrons and hole [21,22]. The photo-generated electrons on the conduction band (CB) of $NiCo_2V_2O_8$ can easily migrate towards the surface and create molecular oxygen anion radical (O_2^{*}) from molecular oxygen, while photo-generated holes on the valence band (VB) of $NiCo_2V_2O_8$ can directly oxidize the dye or produce hydroxyl radicals (OH^{*}) from adsorbed water molecules. The active radicals in the photocatalytic phase are OH^{*}, O_2^{*-} and holes. Extremely reactive O_2^{*-} and OH^{*} oxidize the adsorbed dye molecules. In addition, as shown in Fig. 8, active photo-excited electrons and holes chemically degrade the dye molecules and complete the process of degradation [19,22].

Supercapacitor study: The electrochemical experiments were conducted by employing the cyclic voltammetry (CV) and electrochemical impedance spectroscopy (EIS) using a three-electrode cell in 0.1 M HCl at room temperature. The

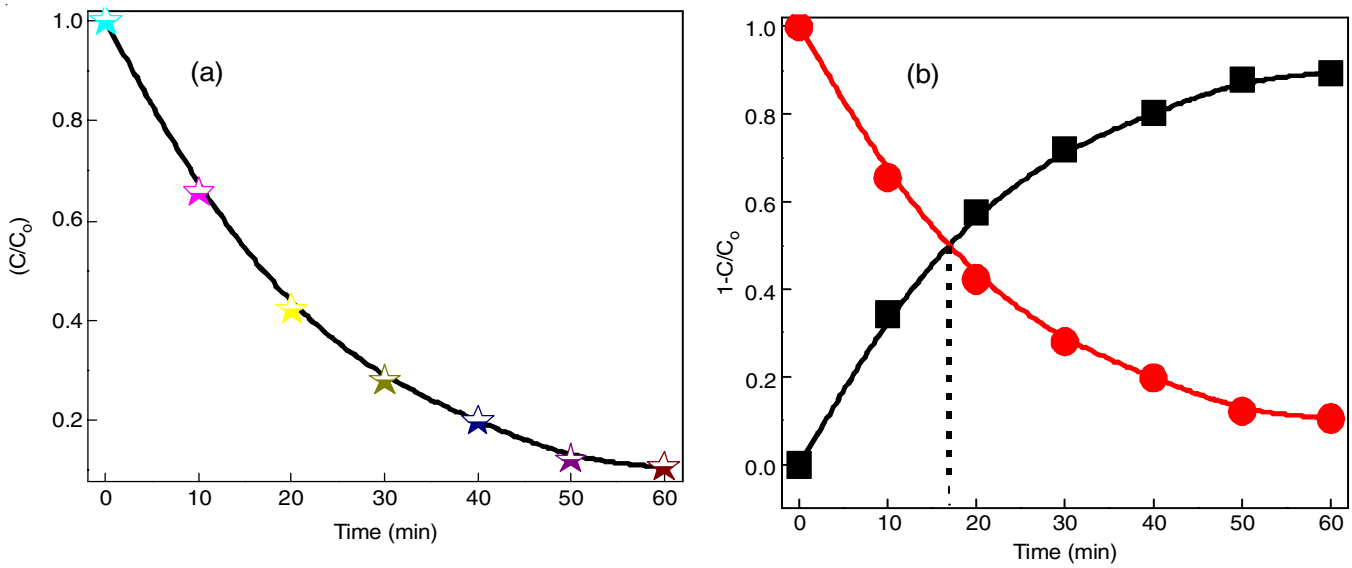

Fig. 7. (a) Plot of C/C$_o$ for the decolorization of MG under UV light illumination, (b) time span of $NiCo_2V_2O_8$ photocatalyst

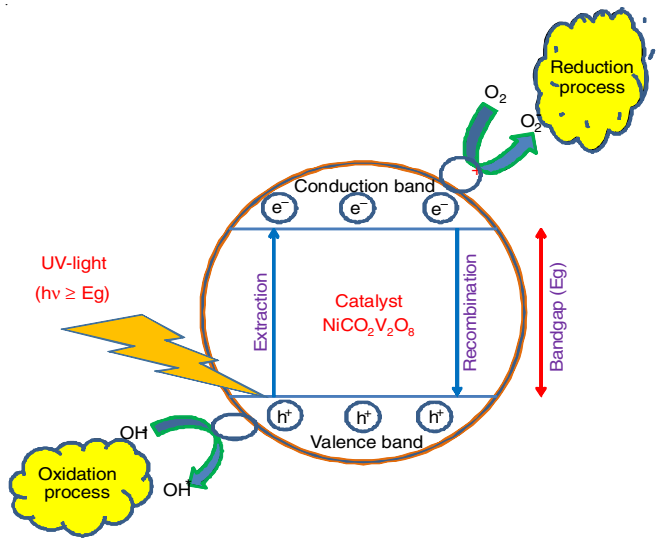

Fig. 8. Mechanism of malachite green decomposition for $NiCo_2V_2O_8$ photocatalyst

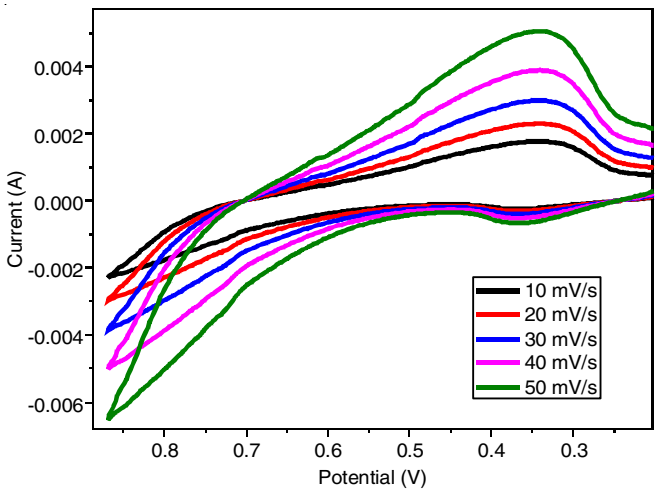

Fig. 9. Cyclic voltammogram of $NiCo_2V_2O_8$ electrode

CV studies provide insight into charge efficiency and reversibility of the electrode reaction. The CV curves of $NiCo_2V_2O_8$ electrode are shown in Fig. 9 (with scan rates varying between 10 and 50 mV/s in 0.1 M HCl). The voltammogram showed a pair of reversible oxidation-reduction peaks confirming the faradaic reactions of the electrode material with the electrolyte ions (Fig. 9) [23].

The CV result of $NiCo_2V_2O_8$ electrode has demonstrated a pseudo-capacitive characteristics. The capacitance of an electrode is dependent on the ionic conductivity of the electrolyte. In order to achieve high power density and large capacitance values, the electrolyte ions must have ionic size less than or equal to the pore size of the working electrode material [24-26]. This is possibly due to the size of the hydrated ions, which greatly influence the ionic conductivity and also the specific capacitance. The specific capacitance of the electrodes was deduced by using eqn. 6 [27]:

$$C_{sp} = \frac{S}{mk\Delta V} \quad (6)$$

where, S = area under the CV curve, m = weight of the deposited material on electrode, ΔV = voltage window, and k = scan rate.

For an electrode, the area under the CV curve depicts its specific capacitance indicating the overall charge (Q) accumulated/stored. It can be concluded that an electrode with comparatively larger area yields a better capacitance at the known mass of electrode material loaded and potential window. Using eqn. 6, the specific capacitance value for the electrode was calculated as 213.8 F g^{-1} in 0.1 M HCl.

The charge transfer characteristics of $NiCo_2V_2O_8$ electrode was explored by acquiring its electrochemical impedance spectrum (Fig. 10) in 0.1N HCl electrolyte (frequency range, 1 Hz –1 MHz and 5 mV amplitude). The impedance spectrum of an electrode displayed a semi-circular pattern with a small diameter at the region of high frequency, which confirms the low charge transfer resistance (R_{ct}) and high capacitance (C)

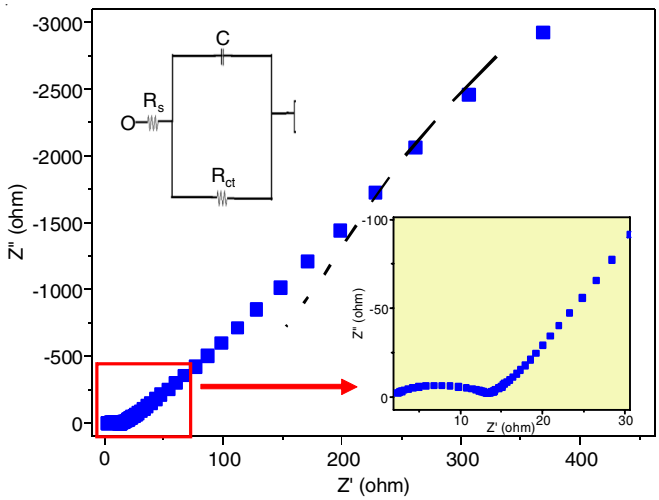

Fig. 10. Nyquist plot of $NiCo_2V_2O_8$ electrode with an equivalent circuit (inset)

of the electrode [27,28]. All the experimentally obtained data are in compliance with the R_{ct} and C values obtained during the equivalent circuit fitting (inset of Fig. 10) for Nyquist plot, as listed in Table-3.

TABLE-3
ELECTROCHEMICAL PARAMETERS FOR $NiCo_2V_2O_8$ ELECTRODE USING FITTING THE EQUIVALENT CIRCUIT

Name of the electrode	Charge-transfer resistance (R_{ct}) (Ω)	Capacitance of double layer (C_{dl}) (F)
$NiCo_2V_2O_8$	56.78	0.00745

Fig. 11a and b shows the galvanostatic charge-discharge (GCD) profile of $NiCo_2V_2O_8$ electrode at 1 A/g current density in 0.1 M HCl solution. The GCD pattern signifies the symmetric charging and discharging curves. Owing to the resistance factor between the interface of electrode and electrolyte, a small IR drop at the point of conversion from charging to discharging can be noticed [28]. The pseudo-capacitance nature of the electrode directly corroborates the coulomb efficiency and high reversibility of faradic ion kinetics, which is clear from the identical GCD patterns of the charging and discharging studies. The specific capacitance $NiCo_2V_2O_8$ electrode from the GCD curve can be estimated using eqn. 7 [27]:

$$C_{sp} = \frac{i\Delta t}{m\Delta v} \quad (7)$$

where, i = applied current, Δt = discharging time, m = mass of the active material loaded onto the substrate and Δv = potential window.

The C_{sp} of $NiCo_2V_2O_8$ electrode at 1 A g^{-1} was calculated to be 218.4 F g^{-1}. This is comparable to the CV results at a current density of 1 A/g with a retention rate of 90.4 % even after 1000 cycles.

The GCD curves for $NiCo_2V_2O_8$ electrode at various current densities are shown in Fig. 11c. The shape of the GCD curves clearly corroborates the electrode behaviour not to be in accordance with that of a pure electric double layer capacitor, but with that of a pseudo-capacitor.

Conclusion

A $NiCo_2V_2O_8$ nanomaterial was synthesized using a hydrothermal route without using any capping agent. The synthesized nanostructures were investigated for their photocatalytic and electrochemical activities. The structural and morphological features of the nanostructures were studied comprehensively using the advanced technical tools. The $NiCo_2V_2O_8$ nanostructures exhibited better photocatalytic activity in the degradation of malachite green dye under UV light irradiation. The cyclic voltammograms revealed that nanomaterial content showed uppermost specific capacitance of 213.8 F g^{-1} in 0.1 M HCl at 10 mV/s scan rate which is near to results obtained from C-D results of 218.4 F g^{-1}. From these results, it is affirmed that $NiCo_2V_2O_8$ nanostructures are better electrochemical and photocatalytic materials best suitable for applications in supercapacitor and energy storage devices as well as in the removal of organic dyes from the wastewater.

ACKNOWLEDGEMENTS

The authors are grateful to DST-SAIF Cochin, Cochin, India for the TEM analysis.

CONFLICT OF INTEREST

The authors declare that there is no conflict of interests regarding the publication of this article.

REFERENCES

1. A.M. Andwari, A. Pesiridis, S. Rajoo, R. Martinez-Botas and V. Esfahanian, *Renew. Sustain. Energy Rev.*, **78**, 414 (2017); https://doi.org/10.1016/j.rser.2017.03.138
2. Z. Yufei, L. Laiquan, S. Haiquan, H. Wei and D. Xiaochen, *J. Mater. Chem. A Mater. Energy Sustain.*, **2015**, 43 (2015); https://doi.org/10.1039/C5TA03899E

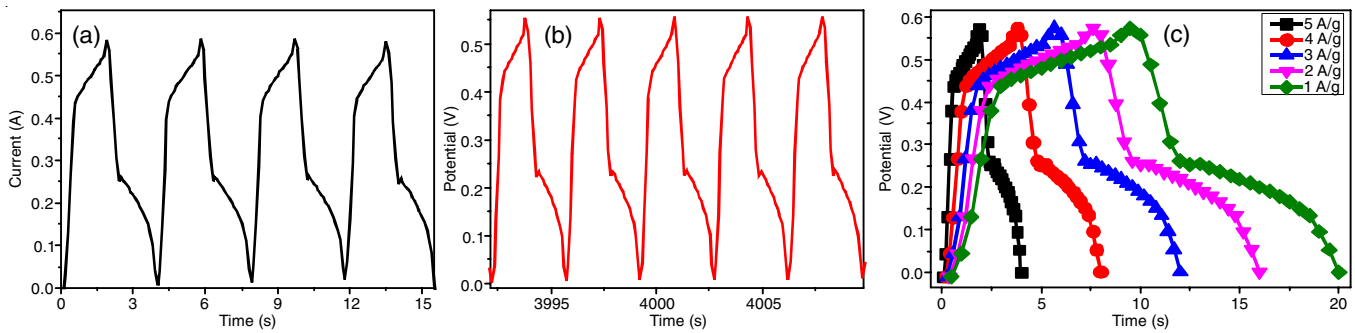

Fig. 11. Galvanostatic charge-discharge curves $NiCo_2V_2O_8$ electrode (a) 1st four cycles (b) 1000th cycle and (c) at various current density

3. G. Wang, L. Zhang and J. Zhang, *Chem. Soc. Rev.*, **41**, 797 (2012); https://doi.org/10.1039/C1CS15060J
4. P. Venkateswarlu, E. Umeshbabu, U.N. Kumar, P. Nagaraja, P. Tirupathi, G. Ranga Rao and P. Justin, *J. Colloid Interface Sci.*, **503**, 17 (2017); https://doi.org/10.1016/j.jcis.2017.05.007
5. G. Rajeshkhanna, E. Umeshbabu, P. Justin and G. Ranga Rao, *Int. J. Hydrogen Energy*, **40**, 12303 (2015); https://doi.org/10.1016/j.ijhydene.2015.06.046
6. Y. Dai, Q. Li, S. Tan, Q. Wei, Y. Pan, X. Tian, K. Zhao, X. Xu, Q. An, L. Mai and Q. Zhang, *Nano Energy*, **40**, 73 (2017); https://doi.org/10.1016/j.nanoen.2017.08.011
7. N.R. Lakshmana, P. Justin and N.T. Bala, *J. Adv. Sci. Technol.*, **29**, 10012 (2020).
8. X. Liu, Y. Hu, G. Jia, H. Zhang, H. Jiang and C. Li, *J. Mater. Chem. A Mater. Energy Sustain.*, **4**, 12030 (2016); https://doi.org/10.1039/C6TA03335K
9. E. Kianfar, *Microchem. J.*, **145**, 966 (2019); https://doi.org/10.1016/j.microc.2018.12.008
10. D. McNulty, G. Collins and C. O'Dwyer, *J. Mater. Chem. A Mater. Energy Sustain.*, **6**, 18103 (2018); https://doi.org/10.1039/C8TA05327H
11. D. McNulty, D. Buckley and C. O'Dwyer, *J. Electrochem. Soc.*, **161**, A1321 (2014); https://doi.org/10.1149/2.0601409jes
12. D. McNulty, D.N. Buckley and C. O'Dwyer, *J. Solid State Electrochem.*, **20**, 1445 (2016); https://doi.org/10.1007/s10008-016-3154-2
13. J. Zhang, B. Yuan, S. Cui, N. Zhang, J. Wei, X. Wang, D. Zhang, R. Zhang and Q. Huo, *Dalton Trans.*, **46**, 3295 (2017); https://doi.org/10.1039/C7DT00435D
14. C.R. Ravikumar, P. Kotteeswaran, A. Murugan, V. Bheema Raju, M.S. Santosh, H.P. Nagaswarupa, H. Nagabhushana, S.C. Prashantha, M.R. Anil Kumar and K. Gurushantha, *Mater. Today Proc.*, **4**, 12205 (2017); https://doi.org/10.1016/j.matpr.2017.09.151
15. C. O'Dwyer, G. Gannon, D. McNulty, D.N. Buckley and D. Thompson, *Chem. Mater.*, **24**, 3981 (2012); https://doi.org/10.1021/cm302648h
16. C. Pratapkumar, S.C. Prashantha, H. Nagabhushana, M.R. Anilkumar, C.R. Ravikumar, H.P. Nagaswarupa and D.M. Jnaneshwara, *J. Alloys Compd.*, **728**, 1124 (2017); https://doi.org/10.1016/j.jallcom.2017.09.058
17. M.A.S. Amulya, H.P. Nagaswarupa, M.R.A. Kumar, C.R. Ravikumar and K.B. Kusuma, *J. Phys. Chem. Solids*, **148**, 109661 (2021); https://doi.org/10.1016/j.jpcs.2020.109661
18. K. Anandan and V. Rajendran, *Mater. Sci. Eng. B*, **199**, 48 (2015); https://doi.org/10.1016/j.mseb.2015.04.015
19. M. Iqbal, A. Saeed and R.G. Edyvean, *Chem. Eng. J.*, **225**, 192 (2013); https://doi.org/10.1016/j.cej.2013.03.079
20. 20 M.R.A. Kumar, B. Abebe, H.P. Nagaswarupa, H.C.A. Murthy, C.R. Ravikumar and F.K. Sabir, *Sci. Rep.*, **10**, 1249 (2020); https://doi.org/10.1038/s41598-020-58110-7
21. V.G. Dileepkumar, P.S. Surya, C. Pratapkumar, R. Viswanatha, C.R. Ravikumar, M.R. Anil Kumar, H.B. Muralidhara, I.M. Al-Akraa, A.M. Mohammad, Z. Chen, X.-T. Bui and M.S. Santosh, *J. Environ. Chem. Eng.*, **8**, 104005 (2020); https://doi.org/10.1016/j.jece.2020.104005
22. C.R. Ravi kumar, P. Kotteeswaran, V.B. Raju, A. Murugan, M.S. Santosh, H.P. Nagaswarupa, S.C. Prashantha, M.R.A. Kumar and M.S. Shivakumar, *J. Energy Storage*, **9**, 12 (2017); https://doi.org/10.1016/j.est.2016.11.001
23. A.N. Kumar, D.M. Jnaneshwara, C.R. Ravikumar, M.R.A. Kumar, H.C.A. Murthy, T.R.S. Shekhar and A.A. Jahagirdar, *Sensors Int.*, **2**, 100076 (2020); https://doi.org/10.1016/j.sintl.2020.100076
24. B. Abebe, C.R. Ravikumar, E.A. Zereffa, A. Naveen Kumar and H.C.A. Murthy, *Inorg. Chem. Commun.*, **123**, 108343 (2021); https://doi.org/10.1016/j.inoche.2020.108343
25. B. Avinash, C.R. Ravikumar, M.R.A. Kumar, H.P. Nagaswarupa, M.S. Santosh, A.S. Bhatt and D. Kuznetsov, *J. Phys. Chem. Solids*, **134**, 193 (2019); https://doi.org/10.1016/j.jpcs.2019.06.012
26. M.A.S. Amulya, H.P. Nagaswarupa, M.R.A. Kumar, C.R. Ravikumar, S.C. Prashantha and K.B. Kusuma, *Surface Sci. Adv.*, **1**, 100023 (2020); https://doi.org/10.1016/j.apsadv.2020.100023
27. R. Ranjitha, K.N. Meghana, V.G.D. Kumar, A.S. Bhatt, B.K. Jayanna, C.R. Ravikumar, M.S. Santosh, H. Madhyastha and K. Sakai, *New J. Chem.*, **45**, 796 (2021); https://doi.org/10.1039/D0NJ05268J
28. A.I. Inamdar, Y.S. Kim, J.S. Sohn, H. Im, H. Kim, D.Y. Kim, R.S. Kalubarme and C. Park, *J. Korean Phys. Soc.*, **59**, 145 (2011); https://doi.org/10.3938/jkps.59.145